ADVANCED FUNCTIONAL MATERIALS
www.afm-journal.de

Piezoelectric Gold: Strong Charge-Load Response in a Metal-Based Hybrid Nanomaterial

Charlotte Stenner, Li-Hua Shao, Nadiia Mameka, and Jörg Weissmüller*

Impregnating the pores of nanoporous gold with aqueous electrolyte yields a hybrid nanomaterial with two separate and interpenetrating charge transport paths, electronic conduction in the metal and ionic conduction in the electrolyte. As the two paths are capacitively connected, space-charge layers along the internal interfaces are coupled to electric potential differences between the paths and can be controlled or detected thereby. The present experiments show that the space charge couples to mechanical deformation of the hybrid material, so that external loading generates an electric current. The electric signal originates from charge displacement along the entire internal interface; the signal is particularly robust since the interface area is large. The charge transfer in response to load constitutes a piezoelectric response, yet the mechanism is quite different to classic piezoelectricity. The analysis in this work predicts links between electromechanical coupling parameters for strain sensing and actuation, which are in excellent agreement with the experiment.

1. Introduction

Piezoelectricity (from piezo (πι ζω) greek for to squeeze or press, and electron (γεκτρον) for amber, a source of charge) describes the phenomenon that certain materials displace electric charge when subjected to an external load.[1] In *conventional* piezoelectric crystals, electricity couples to mechanics since strain polarizes each crystallographic unit cell. The polarization is inherently linked to an internal electric field in the crystal. Since the conduction electrons in a metal screen electric fields, preventing *bulk* polarization, it is generally taken for granted that piezoelectricity is restricted to insulators. Yet, the *interface* between a metal and an ionic conductor (an "electrode surface" in electrochemistry) can be polarized. Furthermore, the electric potential of an electrode couples to elastic strain.[2,3] The contribution of the *external* surface is typically negligible for the behavior of a macroscopic solid body. However, nanoporous metals can be designed to contain an extremely large *internal* surface area. Impregnating a nanoporous metal with electrolyte creates a hybrid material with internal electrode surfaces separated by only few nm.[4] Such materials contain an almost homogeneous distribution of polarizable sites. Here, we show that a hybrid material based on nanoporous gold indeed reacts to mechanical loading by displacing electric charge. In other words, a metal-based material may behave phenomenologically similar to a piezoelectric solid.

Nanoporous metal samples with uniform network of nanoscale "ligaments" can be created by dealloying.[5–7] Monolithic samples with dimension of mm or cm and good mechanical properties can be made,[8] while ligament sizes, L, can reach down to 5 nm.[9,10] Previous work on nanoporous metal actuators exploits the above-mentioned polarization of electrode surfaces. The polarization changes the acting capillary force ("surface stress"), and consequently these materials respond to potential variation by macroscopic expansion or contraction.[4,10–13]

It is well established that the coupling phenomena which locally connect capillary forces to the electric potential at metal electrode surfaces can be inverted: If electric charging affects the capillary force, then mechanical straining changes the electrode potential.[2,3,14] One may envisage that a similar inverse phenomenon exists at the materials' scale: In view of the actuation phenomena, the mechanical deformation of a nanoporous-metal-based hybrid material should prompt an electric potential change or charge displacement. Here, we explore this concept in experiments on nanoporous gold (NPG) and we verify the underlying thermodynamic description that links the novel sensing phenomena to established observations on actuation with nanoporous metal. Comparing the sensing characteristics to those of a high-performance piezoceramic, we advertize the large charge transfer when NPG is strained.

2. Electromechanical Coupling

We start out by summarizing the theory of electrochemical actuation and sensing with nanoporous solids. As detailed in

C. Stenner, Dr. L.-H. Shao, Prof. J. Weissmüller
Institute of Materials Physics and Technology
Hamburg University of Technology
21073 Hamburg, Germany
E-mail: charlotte.stenner@tuhh.de
Dr. L.-H. Shao
Institute of Solid Mechanics
Beihang University (BUAA)
Beijing 100191, P. R. China
Dr. N. Mameka, Prof. J. Weissmüller
Institute of Materials Research
Materials Mechanics
Helmholtz-Zentrum Geesthacht
21502 Geesthacht, Germany

DOI: 10.1002/adfm.201600938

Ref. [14], we consider electrode surfaces which can be elastically strained as well as electrically polarized.

Charging an electrode surface leads to a change in surface stress, f, by $\delta f = \varsigma \delta q$ with $\varsigma = \mathrm{d}f/\mathrm{d}q|_e$ the electrocapillary coupling parameter, e the tangential elastic area strain (relative change in area), and q the superficial charge density (charge per area). The charge-induced change in surface stress modifies the compensating bulk stresses, the average of which depends on the geometry of the microstructure through the orientation distribution of the surfaces.[15] The modification of the bulk stress entails a strain throughout the bulk. In network solids, such as NPG, the effective macroscopic linear strain, ε^*, (relative change in sample length) is governed by a projection of the local strains into the direction of the load-bearing paths in the network. The effective strain then obeys[16]

$$\delta\varepsilon^* = -\frac{2\alpha\theta}{9K}\delta f \tag{1}$$

with K the bulk modulus of the solid phase, α the specific surface area (area per volume of the solid phase), and Θ a dimensionless parameter that depends on the microstructure and on Poisson's ratio, ν, of the solid.

Figure 1a,b illustrates the microstructure of NPG and of an idealized model geometry in which the "ligaments" of the network are approximated as cylindrical wires. For this idealized geometry one has $\Theta = \frac{3}{2}(1-\nu)/(1-2\nu)$ or ≈7.0 (for gold, ν = 0.44), whereas a numerical simulation with more realistic geometry for NPG finds Θ = 5.5.[16]

A thermodynamic Maxwell relation equates the charge-response of f to the response of the electrode potential, E, to tangential strain, that is, $\mathrm{d}E/\mathrm{d}e|_q = \mathrm{d}f/\mathrm{d}q|_e = \varsigma$.[2,3,14] Figure 1a illustrates the consequence: Since charging leads to expansion or contraction of the ligaments in NPG, one can expect that straining leads to accumulation of charge (at constant potential) or to potential variation (at open circuit and constant charge). Yet, the microscopic picture presented so far does not afford a precise estimate of the potential- or charge response to strain at the materials' level. This is because the macroscopic deformation of a solid network, such as Figure 1b, results in a heterogeneous local strain field, so that e differs from the macroscopic strain and is nonuniform. We shall now examine actuation and sensing in a macroscopic approach that points toward a solution for the problem.

Here, we consider the porous solid sample as an effective medium, ignoring the microstructure. The total sample volume

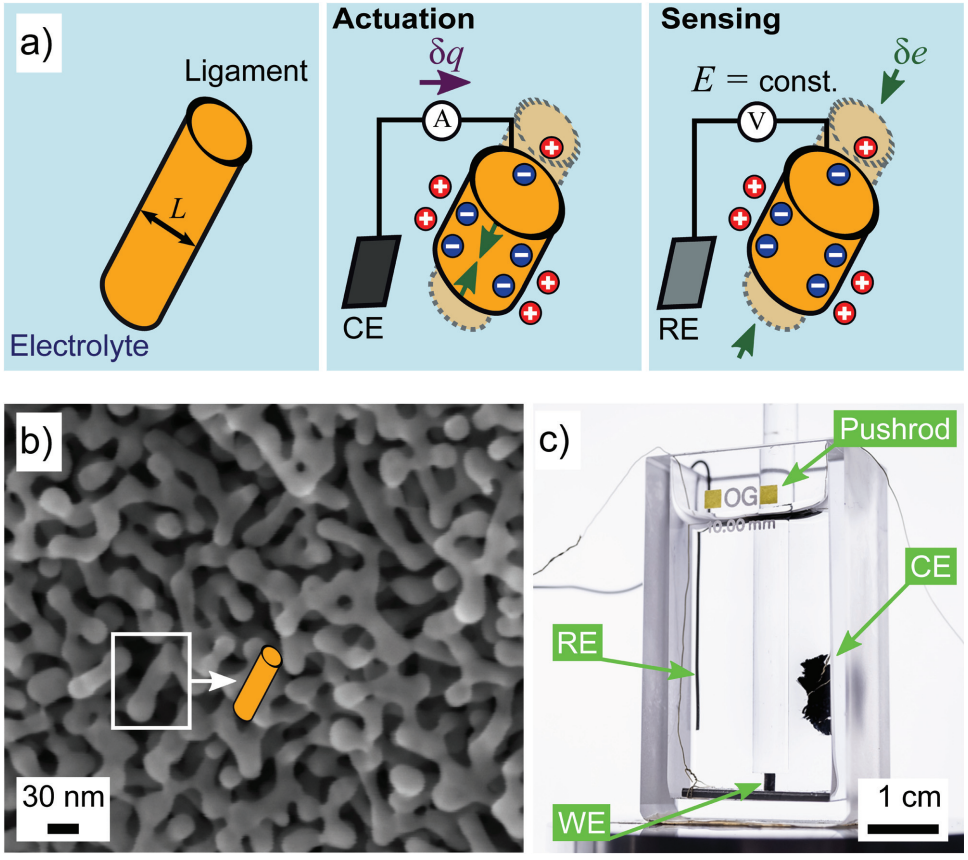

Figure 1. Sensing and actuation with nanoporous metal. a) Schematic illustration. Left, circular wire, representing a ligament of size L in electrolyte. Centre, actuation: Imposing a variation in charge, δq, results in contraction (green arrows) of the wire. A strain is acting on the ligament (green arrows). Right, sensing: Imposing an axial strain, δe, leads to the spontaneous accumulation of electric charge at the wire surface, if a constant potential is applied. b) SEM image of a NPG sample. Note the similarity between the ligament geometry and the circular wire (sketch) of the model. c) Experimental setup: Electrochemical cell installed in DMA test machine. RE, CE, and WE denote reference, counter, and working electrode, respectively. Fused-silica pushrod transfers load to the sample.

(solid and pores) in the strain-free reference state is denoted by V and the net electric charge by Q. An uniaxial external traction, T (load per area of sample cross-section), is allowed for so that mechanical work can be done through the elastic linear strain ε^* in load direction. The net Helmholtz-type free energy, $\mathfrak{F}$, then depends on the constant V and on the state variables ε^* and Q. We express $\mathfrak{F}$ in terms of volume-specific quantities, $\mathfrak{F} = V\Psi\left(q^{\mathrm{V}}, \varepsilon^*\right)$ with $q^{\mathrm{V}} = Q/V$ the volume-specific charge and Ψ a free energy density function. The fundamental equation for Ψ is

$$\mathrm{d}\Psi = E\mathrm{d}q^{\mathrm{V}} + T\mathrm{d}\varepsilon^* \tag{2}$$

An effective strain-charge (actuation) coefficient A^* may be defined as

$$A^* = \left.\frac{\mathrm{d}\varepsilon^*}{\mathrm{d}q^{\mathrm{V}}}\right|_T \tag{3}$$

and based on Equation (1) one readily finds

$$A^* = -\frac{2\zeta}{9K\varphi}\Theta \tag{4}$$

with φ the volume fraction of the solid phase.

In the following instance of the triple product rule

$$\left.\frac{\mathrm{d}T}{\mathrm{d}q^{\mathrm{V}}}\right|_{\varepsilon^*} = -\left.\frac{\mathrm{d}T}{\mathrm{d}\varepsilon^*}\right|_{q^{\mathrm{V}}} \left.\frac{\mathrm{d}\varepsilon^*}{\mathrm{d}q^{\mathrm{V}}}\right|_T \tag{5}$$

one can identify the effective potential-strain coupling coefficient (potential variation per strain at open circuit),

$$\zeta^* = \left.\frac{\mathrm{d}E}{\mathrm{d}\varepsilon^*}\right|_{q^{\mathrm{V}}} \tag{6}$$

via the Maxwell relation

$$\left.\frac{\mathrm{d}T}{\mathrm{d}q^{\mathrm{V}}}\right|_{\varepsilon^*} = \left.\frac{\mathrm{d}E}{\mathrm{d}\varepsilon^*}\right|_{q^{\mathrm{V}}} \tag{7}$$

The (open circuit) effective Young's modulus Y^* is defined as

$$Y^* = \left.\frac{\mathrm{d}T}{\mathrm{d}\varepsilon^*}\right|_{q^{\mathrm{V}}} \tag{8}$$

Therefore, Equation (5) implies

$$\zeta^* = -Y^*A^* \tag{9}$$

This equation, which follows from the fundamental Equation (2) without further assumptions, relates the potential-strain coupling coefficient ζ^* to the actuation coefficient A^*. Thus it can be used to infer, based on actuation experiments, the magnitude of electric (sensing) signals generated in response to load. Furthermore, the mechanics of porous media offers a discussion of Y^* that connects to the issue of local versus macroscopic strain (see Section 4 below).

It is also of interest to estimate the coupling between the net charge on a nanoporous body and strain. Denoting by $C = \mathrm{d}Q/\mathrm{d}E$ and $c = \mathrm{d}q/\mathrm{d}E$ the *net* differential sample capacity and the *local* differential capacitance (capacity per area) of the metal surface, respectively, this coupling emerges as

$$\left.\frac{\mathrm{d}Q}{\mathrm{d}\varepsilon^*}\right|_E = -\left.\frac{\mathrm{d}Q}{\mathrm{d}E}\right|_{\varepsilon^*} \left.\frac{\mathrm{d}E}{\mathrm{d}\varepsilon^*}\right|_Q = -C\,\zeta^* = c\alpha\varphi VY^*A^* \tag{10}$$

For reference below, we advertize the fact that the charge which is transferred per strain here scales with the actuator volume. This distinguishes nanoporous strain sensors from piezoceramic ones, for which the charge scales with the cross-sectional area.

An important figure of merit of piezoceramic sensors, the longitudinal piezoelectric coefficient d_{33}, is defined as charge displaced per load ($F = aT$ with a the cross-sectional area; tensile loads are positive). For a nanoporous body of cross-sectional area a and thickness t, the respective coupling strength is obtained as indicated in the following sequence of equations

$$\left.\frac{\mathrm{d}Q}{\mathrm{d}F}\right|_E = \frac{1}{a}\left.\frac{\mathrm{d}Q}{\mathrm{d}T}\right|_E = \frac{1}{a}\left.\frac{\mathrm{d}Q}{\mathrm{d}\varepsilon^*}\right|_E \left.\frac{\mathrm{d}\varepsilon^*}{\mathrm{d}T}\right|_E \approx -\frac{c\alpha\varphi\zeta^*}{Y^*}t \tag{11}$$

where the last step used Equation (10) and the approximation $Y^* = \left.\frac{\mathrm{d}T}{\mathrm{d}\varepsilon^*}\right|_{q^{\mathrm{V}}} \approx \left.\frac{\mathrm{d}T}{\mathrm{d}\varepsilon^*}\right|_E$.[17] The charge-load coefficient scales with the thickness, whereas d_{33} of a piezoceramic is a materials parameter, independent of the geometry.

3. Results

Millimeter-sized cylindrical NPG samples infiltrated with electrolyte were investigated in situ via a dynamic mechanical analyzer (DMA) test machine in an electrochemical cell as shown in Figure 1c. Actuation experiments were performed at constant load while sweeping the potential cyclically and simultaneously measuring the resulting effective strain ε^*. For sensing experiments, the sample was strained cyclically (with the amplitude $\hat{\varepsilon}^*$ and at a constant offset of ε_0^*) and the corresponding electrical signals were recorded at constant potential. After each sensing/actuation experiment the effective Young's modulus Y^* was determined. A more detailed description of the experimental procedures is given in the Experimental Section.

Representative results for electrochemical actuation are compiled in **Figure 2**. In each experiment, the effective strain ε^* was measured during five subsequent potential scans (–0.1 to 0.4 V at scan rate 2 mV s^{-1}). The contact force of the DMA pushrod resulted in a small constant applied stress, 0.11 MPa. Figure 2a shows that the sign of the potential-strain coupling, expansion during positive-going potential scans, agrees with previous actuation experiments with NPG.[18–20]

The effective strain-charge coefficient A^* was computed by means of Equation (3) using data such as Figure 2a. Averages were taken over 5 cycles, separately for positive and negative-going sweeps, and Figure 2b plots the averaged strain versus q^{V}. Linear regression of this data suggests $A^* = 0.0471 \pm 0.0004$ $\mathrm{mm^3\,C^{-1}}$. On average over the three samples

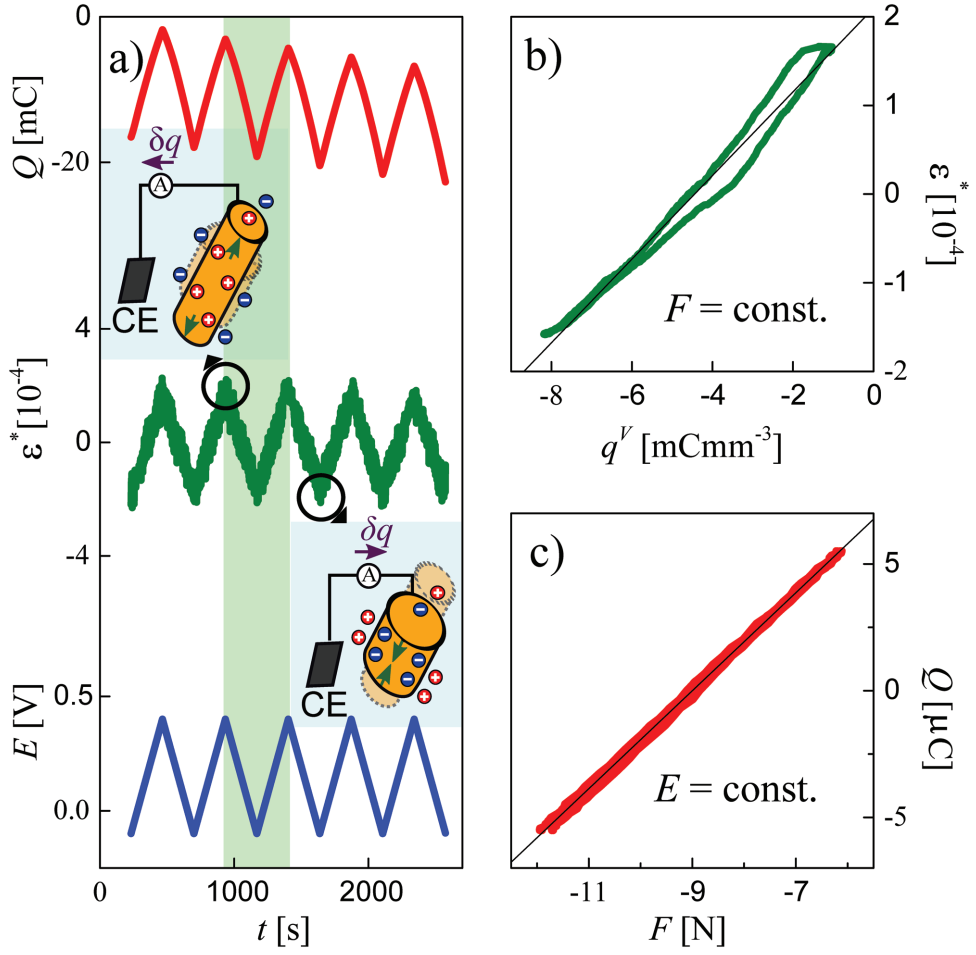

Figure 2. Actuation and quasi-static sensing measurements. a) Five representative potential sweeps. The effective strain ε^* (green line) and the charge Q (light red) increase or decrease, respectively, with increasing or decreasing potential (blue line, measured vs a Ag/AgCl pseudoreference electrode). Sketches illustrate the electromechanical coupling in a wire-shaped ligament. b) Averaged effective-strain ε^* versus volumetric charge density q^V for the data of (a). c) Charge Q versus applied force amplitude F (light red line; note that compressive load is negative) in a quasi-static sensing experiment at $\omega/2\pi = 10$ mHz and at constant applied potential. Thin black lines in panels (b) and (c) represent linear fits.

in this study, we found $A^* = 0.0475 \pm 0.0010$ mm^3 C^{-1}. The small variance implies an excellent sample-to-sample reproducibility.

Before and after each actuation measurement the effective Young's modulus Y^* was determined as the storage modulus in the DMA. It was found that Y^* remained constant during the measurements. The average over all samples was $Y^* = 450 \pm 50$ MPa, consistent with what has been reported for comparable NPG samples.[21]

The sensing experiments were performed with an electrode bias potential at $E = 0.4$ V versus the Ag/AgCl pseudoreference electrode in the capacitive regime. Quasi-static sensing experiments with the load modulated at frequency 10 mHz explored the coupling, $dQ/dF|_E$, between net charge on the sample and external load near equilibrium. The sample was prestrained by a static force $F_0 = -9.2$ N (negative-valued for compression), whereas the force amplitude $\hat{F}$ was 2.85 N. Figure 2c shows that the charge varies linearly with strain, and linear regression supplies $dQ/dF|_E = 1.933 \pm 0.003$ μC N^{-1}.

Figure 3 compiles representative oscilloscope traces (without further amplification) for two separate sensing experiments at higher frequency. While the strain (black graph at bottom of Figure 3a) was modulated at the frequency $\omega/2\pi = 5$ Hz, we recorded the potential variation under conditions of zero current. That is the blue graph at the top of Figure 3a. Next, we fixed the potential and recorded the current variation during an identical strain cycle. That is the red graph in the center of the figure. It can be seen that strain amplitudes in the order of 1% prompt readily measurable variations in either potential or current, with amplitudes in the order of 100 μV and 10 μA, respectively. The potential variation is slightly phase shifted with respect to the strain, yet the overall trend is negative-going potential when the sample is elongated, consistent with the trends from the actuation experiment and from the quasi-static sensing experiment.

Additional sensing experiments explored the dependence of the amplitudes $\hat{E}$ and $\hat{I}$ on the applied strain amplitude $\hat{\varepsilon}^*$ Figure 3c,d shows results at frequency 20 Hz. A linear variation in both instances, with a high sample-to-sample reproducibility of the slopes.

Next, we explore whether the signal strength from the quasi-static actuation measurements is quantitatively consistent with

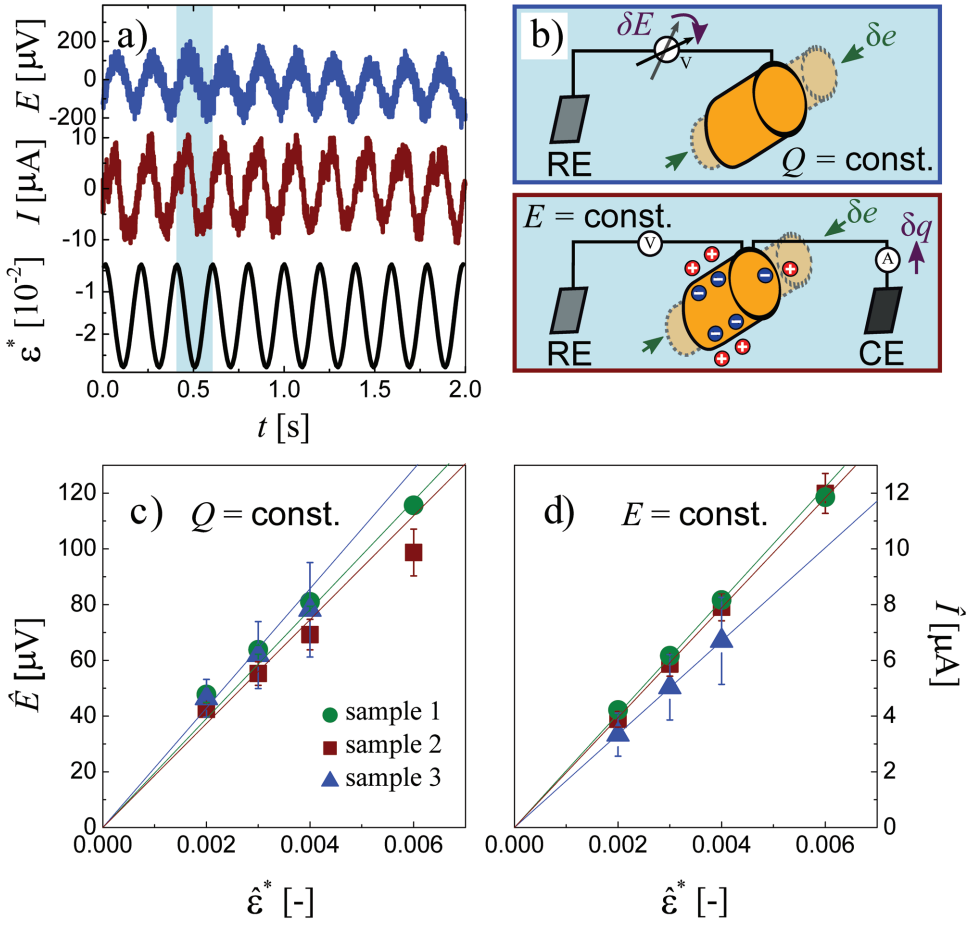

Figure 3. Electric signals in a sensing experiment. a) Oscilloscope traces of potential (blue) and current (red) modulation due to cyclic strain (black) at frequency $\omega/2\pi = 5$ Hz. b) Schematics of circular wire under compression, illustrating the experiments. Top: Strain-induced potential modulation at constant charge results in blue graph of (a), whereas strain-induced charge modulation (bottom) corresponds to red graph in panel (a). c,d) Potential amplitude $\hat{E}$ and current amplitude $\hat{I}$, respectively, versus strain amplitude $\hat{\varepsilon}^*$. Note the linear correlation. Measurements (c) and (d) were performed at $\omega/2\pi = 20$ Hz. Colors and markers indicate results for separate samples.

that of the sensing experiments at 20 Hz. As the basis for the comparison, we choose the potential-strain coupling parameter ς^*, since Equation (9) shows how the parameter can be alternatively determined from the sensing experiment as the strain-derivative of the potential at constant charge (Figure 3c), or from the actuation experiment as the product of effective Young's modulus and actuation coefficient (Figure 2b). The two sets of values for ς^* are shown in **Table 1**, for experiments with three different samples. Table 1 underlines the high sample-to-sample reproducibility in ς^*. Even more importantly, the sets of coefficients determined from sensing coincide, within error bars, with those determined from actuation. This observation provides strong support for our analysis of the sensing and actuation mechanism in terms of electrocapillary coupling, see Section 2 above.

Table 1 also lists net quasi-static capacities, C, and the ensuing (see the Experimental Section) net surface areas, S. All three samples had identical mean ligament size; the different C and S are consistent with the slightly different macroscopic volumes. The capacity per volume is ≈20 F cm^{-3}, well consistent with previous reports on NPG-based supercapacitors.[22] At 40–50 mF, the net capacities are high, emphasizing the extremely large internal surface area and the abundance of polarizable sites in the hybrid material.

It is also of interest in how far the charge transfer is affected by the frequency. We used the potentiostat's impedance

Table 1. Effective potential-strain coupling coefficients for three separate samples and obtained in two independent ways: $\varsigma^* = -Y^*A^*$ is obtained from quasi-static actuation experiments and Young's modulus via Equation (9); $\varsigma^* = \hat{E}/\hat{\varepsilon}|_{q^v}$ is obtained from potential and strain amplitudes in sensing experiments at constant potential and at frequency 20 Hz. Note the agreement between the results of the two independent approaches, as well as the sample-to-sample reproducibility. Also shown: Net capacity, C, and net surface area, S, of each sample.

Sample	C [mF]	S [cm^2]	$\varsigma^* = -Y^*A^*$ [mV]	$\varsigma^* = \hat{E}/\hat{\varepsilon}^*|_{q^v}$ [mV]
1	51.6 ± 1.3	1300	−18.4 ± 2.1	−20.9 ± 1.7
2	46.1 ± 0.3	1150	−21.2 ± 1.6	−21.8 ± 2.0
3	41.8 ± 0.2	1050	−21.1 ± 1.9	−21.1 ± 2.1

module for imposing a 20 Hz potential modulation and determined an effective capacity from the ratio of current- and potential amplitudes, $C = \hat{I}/\omega\hat{E}$. This yielded $C_{20\mathrm{Hz}} = 1.02$ mF, 50-fold less than the quasi-static capacity (Table 1). Next, we applied a strain modulation and measured separately $\hat{I}$ at constant E as well as $\hat{E}$ at constant Q. With these values and the same relation as before, C emerges as 0.88 mF. The two values agree well, indicating that a reduced charge transfer of the sensor at finite frequency can be understood as the result of the electrochemical impedance and, hence, of the ionic transport resistance in the pores. Computing $\mathrm{d}Q/\mathrm{d}F|_E$ at 20 Hz from the load- and current amplitudes of Figure 3c and averaging over the three samples yields 31 nC N^{-1}. As an independent approach, Equation (11), using ς^* from Table 1 and C from the sensing experiment yields $\mathrm{d}Q/\mathrm{d}F|_E = 35$ nC N^{-1}, again in good agreement.

4. Discussion

As the key finding of this study, nanoporous gold (NPG) samples wetted by electrolyte respond to elastic mechanical deformation similarly to piezoelectric solids, namely by exhibiting readily measurable potential changes and by actively generating electric current. Section 2 explains why this behavior is expected based on the phenomenon of electrocapillary coupling at metal surfaces: A macroscopic elastic strain of the NPG body causes local elastic deformation at the surfaces of the internal ligament network. The ensuing local variation of potential or charge-density is governed by the electrocapillary coupling parameter ς. The efficiency of the nanoporous body in generating electric signals in response to deformation depends on the magnitude of ς, on the net area of the surface, and on the efficiency with which macroscopic deformation translates into a local tangential strain at each segment of surface.

In a macroscopic picture of actuation and active strain sensing with NPG, we have defined two parameters that afford a quantification of the material's performance. The actuation coefficient A^* measures strain per charge in actuation, whereas the sensing coefficient ς^* measures potential variation per strain. Equation (9) predicts a link between the two coefficients that also involves the effective Young's modulus, Y^*, of the porous material. We have independently measured each of these three parameters and found the results in excellent agreement with Equation (9). This confirms our phenomenological description of the effective materials behavior.

The above conclusion is further confirmed by comparison of the experimental value of A^* (strain per charge density) to the prediction in Equation (4), which is based on the local electrocapillary coupling strength at the surface and on the local elastic response in the bulk of the ligaments. With $K = 217$ GPa,[23] $\Theta = 5.5$,[16] $\varsigma = -2.0$ V,[3,24–27] and $\varphi = 0.26$, Equation (4) predicts $A^* = 0.0433$ mm^3 C^{-1}, which agrees well with the mean experimental $A^* = 0.0475$ mm^3 C^{-1}. The agreement confirms that the sensing and actuation behavior are both manifestations of the same microscopic coupling process, quantified by the local electrocapillary coupling parameter ς.

Our discussion so far concerns actuation experiments, which use switching times of several minutes and which thereby explore a quasi-static scenario. Sensing requires charge transfer at higher frequency. Our experiments at 20 Hz show an effective capacity considerably below the quasi-static one. The need for ionic transport in the pore space provides a natural explanation of this observation, which is also supported by electrochemical impedance spectroscopy on NPG.[28] Importantly, however, the data in Table 1 show the potential variation during constant-charge sensing at 20 Hz in quantitative agreement with the quasi-static actuation results, thereby supporting the notion of the material as an active strain sensor that provides relevant signals even at finite frequency.

The experimental value of ς^* for the material of our study is -21 ± 2 mV. Thus, a strain of 1% results in a potential variation of 210 μV. This is a much smaller potential variation than what can be reached with piezoceramics. However, NPG active strain sensors are distinguished by their extremely large surface area and, consequently, by their large electric capacity. This implies that readout circuitry in a conceivable application can be comparatively simple and inexpensive, even though the voltage is small.

Our investigation into active sensing with NPG was partly motivated by the expectation that the abundant active sites—which all contribute to the potential change or to the charge displacement—at the extremely large internal surface would make for particularly robust stress or strain sensing. The comparison to a high performance piezoceramic affords an assessment of that expectation; results are summarized in **Figure 4**. The piezoelectric charge-sensor constant d_{33} (longitudinal direction) for lead zirconium titanate (PZT, here: $(Pb_{0.85}Ba_{0.15})_{0.9925}La_{0.005}(Zr_{0.52}Ti_{0.48})O_3$) is 410 pC N^{-1}.[29] The quasi-static measurements

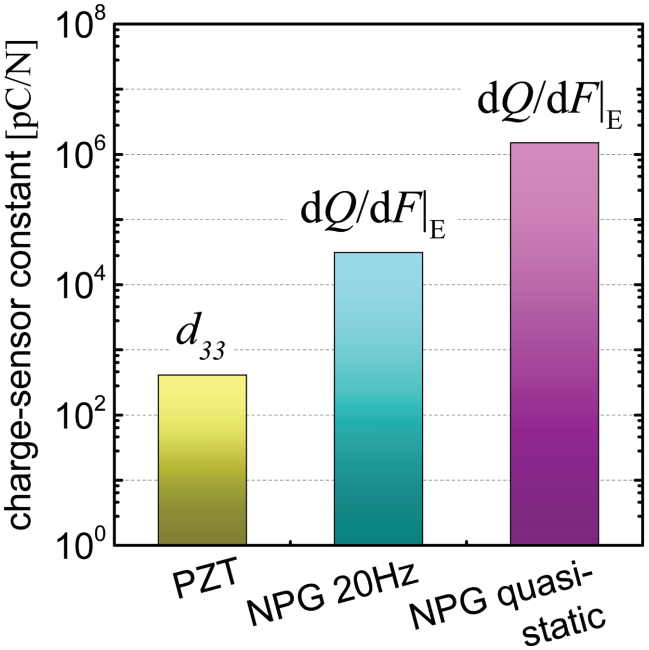

Figure 4. Comparing the charge-load response of nanoporous gold- (NPG-) based hybrid material to that of lead zirconium titanate (PZT). The response $\mathrm{d}Q/\mathrm{d}F|_E$ of NPG at frequency 20 Hz is 75-fold larger than the piezoelectric charge-sensor constant d_{33} of PZT.[29] Under quasi-static conditions, $\mathrm{d}Q/\mathrm{d}F|_E$ of NPG is even higher, almost 4000-fold larger than d_{33} of PZT.

with our material imply a mean (averaged over three samples) longitudinal coupling parameter of $dQ/dF|_E$ = 1.5 μC N^{-1}, almost 4000-fold larger than d_{33} of PZT. The NPG value at 20 Hz, $dQ/dF|_E$ = 31 nC N^{-1}, is fifty times less, but still almost two orders of magnitude larger than that of PZT. Note an important distinction: d_{33} is a materials' constant of a piezoceramic and cannot be adjusted by the design of the sensor geometry. By contrast, the longitudinal coupling parameter of our NPG sensors scales with the thickness. Thus, design of the sensor geometry provides a way of tailoring the electric response of NPG.

Nanoporous-metal-based sensors and actuators exhibit similar (though not in all instances identical, see above) phenomenological behavior as piezoelectric solids: Mechanical loading generates electric charge or voltage, and conversely applied potential or charge generate mechanical deformation. Yet, the underlying microscopic mechanisms differ. In piezoelectric crystals the load induces a symmetry-breaking strain that displaces electric charge in each crystallographic unit cell. The polarization of the lattice leads to a charge accumulation at the *external* sample surface. By contrast, the strain of the porous metal changes the chemical potential of the conduction electrons.[24] A polarization of the electrochemical double-layer at the entire *internal* electrode surface is then required in order to compensate this change and keep the electrode potential a constant. Setting up space-charge layers at internal interfaces throughout the porous material requires long-range charge transport, which limits the efficiency at elevated frequency. On the other hand, the large number of internal interfaces implies that the net amount of charge which is displaced in nanoporous sensors in response to strain is much larger than the charge transferred in piezoceramics.

As mentioned above, the efficiency of sensing or actuation with nanoporous metal depends on how macroscopic deformation couples into local strain at the surfaces of the ligaments. This is a nontrivial issue because the elastic behavior of NPG under uniaxial load may be dominated by ligament bending, so that part of the ligament surfaces are strained in compression while others are in tension. The corresponding electric signals would then partly cancel. For NPG, the link between local and macroscopic elastic behavior has been discussed in terms of the Gibson–Ashby scaling relations for porous solids.[7,30] The scaling relation for Young's modulus is $Y^* = Y\varphi^2$, where Y denotes Young's modulus of the solid phase.[31] By inserting the scaling relation for Y^* and Equation (4) for A^* into Equation (9), accounting for $Y = 3K(1-2\nu)$ in isotropic elastic media, one obtains a prediction for the the effective potential-strain response parameter

$$\varsigma^* = \frac{2}{3}(1-2\nu)\varphi\Theta\varsigma \tag{12}$$

With ν = 0.44[23] and with the values of Θ, ς, and φ as above, Equation (12) suggests ς^* = –240 mV, about one order of magnitude larger than the experimental value. The discrepancy is in fact expected, since the Gibson–Ashby scaling relations are known to overestimate the stiffness of macroscopic NPG samples more than tenfold.[32] Disconnected ligaments, which do not participate in the deformation of the loadbearing skeleton within the solid network, have been suggested as the origin of the discrepancy.[8] This implies that nanoporous solids with an *ideally* interconnected network of ligaments would afford a tenfold enhanced sensing efficiency compared to the present results. One more opportunity for enhancing the performance is by increasing the solid fraction. In view of Equation (12), increasing φ enhances the electromechanical coupling, and at the same time more solid fraction also implies more mechanical strength, which may be beneficial for applications.

5. Conclusion

To summarize, our work demonstrates a novel scheme for active strain-sensing with a hybrid material made of nanoporous-gold and aqueous electrolyte. By cyclic loading of mm-size samples, we obtain reproducible and robust electrical signals, that can be measured via an oscillocope, i.e., without further amplification. The signal amplitudes increase linearly with strain and the effective potential-strain coupling parameter is determined as ς^* = –21 mV. We derive a macroscopic sensing-actuation relation, Equation (9), which achieves excellent agreement with the experimental results from sensing, actuation, and effective elasticity measurements. The basis of our analysis of the material's behavior is the electrocapillary coupling at the pore surfaces in the material. The sensing efficiency indeed agrees well with prediction based on that notion. Due to the extremely large internal surface area, the sensor is able to generate significant electric current in response to strain. The charge-load coupling coefficient of nanoporous gold, $dQ/dF|_{E'}$ is found orders of magnitude larger than the equivalent quantity, d_{33}, in our example for a high performance piezoceramic, PZT.

We have discussed the similarities and distinctions between the charge-load response in our hybrid material and that in conventional piezoelectric solids. In each case, charge couples to load, and elastic strain creates polarization. The nature of the polarizable sites—here the internal interfaces—is fundamentally different. Yet, the key phenomenology that is implied by the term piezoelectricity, namely the displacement of electric charge in response to an external load, is common to both classes of materials. Irrespective of the microscopic nature of the electromechanical coupling, the particularly robust signals suggest that nanoporous metals might be attractive for conceivable applications as active strain-sensing components with high strain-induced charge densities.

6. Experimental Section

Cylindrically shaped NPG samples with diameter 1.2 ± 0.05 and length 2.0 ± 0.05 mm were prepared as described in Ref. [33]. As-prepared samples had a mean ligament size L = 40 ± 10 nm (as found by scanning electron microscopy) and a residual silver content below 1 at%, as determined by energy-dispersive X-ray spectroscopy. The solid volume fraction, as determined from the measured mass and macroscopic volume of the sample, was $\varphi \approx 0.26$.

The quasi-static value of the capacity, C, of each sample was measured via cyclic voltammetry in a small potential window, verifying a linear variation of charging current with potential scan rate as in. Ref. [18]. Before and after each experiment, the net surface area, S, in the sample

was determined by the capacitance ratio method, $S = C/c$,[34] using the double layer capacitance value of a clean Au surface, $c = 40$ μF cm^{-2}.[35]

Actuation and sensing measurements were performed in situ in 0.5 M H_2SO_4 prepared from H_2SO_4 (Suprapur, Merck) and ultrapure water (18.2 MΩ cm) and deaerated with argon. Prior to all measurements the cell was cleaned in Piranha solution and rinsed with ultrapure water. All experiments used an Ag/AgCl pseudoreference electrode, +0.405 V versus the standard hydrogen electrode (SHE), and all potentials of this work are specified versus Ag/AgCl. Carbon cloth served as counter electrode. For electric contact the sample was placed on a Pt plate connected to the potentiostat (Autolab) via a gold wire. The electrochemical cell was mounted in a DMA (BOSE ElectroForce) and the load applied via a fused silica pushrod, see Figure 1c.

Prior to the elastic deformation of the actuation or sensing experiments, all samples were deformed in situ to a plastic strain ≈0.15 at strain rate 10^{-4} s^{-1}. This served to ensure uniform contact at the load surfaces. The samples were then first unloaded and subsequently reloaded to an elastic prestrain $\varepsilon_0^* = 0.015$. The sensing experiments were under strain control at frequency ω, with elastic strain, ε^*, versus time, t, given by

$$\varepsilon^*(t) = \varepsilon_0^* + \hat{\varepsilon}^* \sin(\omega t) \tag{13}$$

Amplitudes $\hat{\varepsilon}^*$ ranged from 0.002 to 0.006. The resulting stresses were well below the yield stress, 13 MPa, for the plastically predeformed samples. Electric signals were processed by a lock-in amplifier (Oxford instruments) using the load cell signal of the DMA as the reference signal.

For potential-strain response measurements, a "delay resistance" R_D = 5 kΩ—inserted between working electrode and potentiostat—increased the time constant of the control electronics, preventing it from compensating the sensing potential variation.[25] The amplitude $\hat{E}$ of the potential response to strain (i.e., $E(t) = \hat{E}\sin(\omega t - \phi)$ with ϕ a phase shift) was determined via the lock-in amplifier from the potential between working and reference electrode. For current–strain response experiments, R_D was removed and the lock-in amplifier used for measuring the amplitude $\hat{I}$ of the current–strain response via the potential drop over a shunt resistance, R_S = 47 Ω, connected in series with the counter electrode.

The actuation measurements were performed directly after sensing measurements, only interrupted by determination of the Young's modulus via DMA. The in situ sequence sensing-DMA-actuation-DMA was repeated five times for each sample. The data shown is based on three samples with identical preparation parameters.

As the electrocapillary coupling at gold surfaces is strongest near the potential of zero charge (pzc),[25,26] all experiments used potentials within the capacitive part of the cyclic voltammogram. Actuation experiments explored the potential range –0.1 to 0.4 V, whereas the bias potential for sensing was 0.4 V. Thus, E was always well negative of the onset potential for OH electrosorption, 0.75 V, and close to the pzc, which has been reported as ≈0.5 V versus SCE[36] (or ≈0.3 V on our Ag/AgCl – based potential scale) for Au (111) in solutions containing $H_2SO_4^{2-}$. Cyclic voltammetry confirmed the capacitive behavior in the potential range of our studies.

A typical sensing-actuation-sensing experiment comprised 1.2×10^5 load cycles in sensing plus 25 actuation cycles. It was found that surface areas were reduced by ≈30% after such experiments. The future strategy to avoid this reduction might be alloying with Pt, which is known to stabilize the structure of np AuPt against coarsening.[9,10]

Acknowledgements

This work was supported by DFG via SFB "M^3", subproject B2. L.-H. Shao was partly supported by National Natural Science Foundation of China (NSFC Grant No. 11572051). A wrong variable symbol below eq.12 was corrected after early view publication on July 25, 2016.

Received: February 22, 2016
Revised: March 22, 2016
Published online: June 8, 2016

[1] A. Ballato, in Ultrasonics Symposium 1996 (Eds.: S. M. B. Levy, M. Schneider), *1996 IEEE Ultrasonics Symposium*, Vol. *1*, IEEE, Piscataway, NJ, USA **1996**, pp. 575.
[2] A. Gokhshtein, *Dokl. Akad. Nauk SSSR* **1969**, *187*, 601.
[3] M. Smetanin, D. Kramer, S. Mohanan, U. Herr, J. Weissmüller, *Phys. Chem. Chem. Phys.* **2009**, *11*, 9008.
[4] J. Weissmüller, R. N. Viswanath, D. Kramer, P. Zimmer, R. Würschum, H. Gleiter, *Science* **2003**, *300*, 312.
[5] R. Li, K. Sieradzki, *Phys. Rev. Lett.* **1992**, *68*, 1168.
[6] J. Erlebacher, M. J. Aziz, A. Karma, N. Dimitrov, K. Sieradzki, *Nature* **2001**, *410*, 450.
[7] J. Weissmüller, R. C. Newman, H.-J. Jin, A. M. Hodge, J. W. Kysar, *MRS Bull.* **2009**, *34*, 577.
[8] N. Mameka, K. Wang, J. Markmann, E. T. Lilleodden, J. Weissmüller, *Mater. Res. Lett.* **2016**, *4*, 27.
[9] J. Snyder, P. Asanithi, A. B. Dalton, J. Erlebacher, *Adv. Mater.* **2008**, *20*, 4883.
[10] H. J. Jin, X. L. Wang, S. Parida, K. Wang, M. Seo, J. Weissmüller, *Nano Lett.* **2010**, *10*, 187.
[11] F. Weigend, J. Weissmüller, F. Evers, *Small* **2006**, *2*, 1497.
[12] E. Detsi, M. S. Sellès, P. R. Onck, J. T. M. De Hosson, *Scr. Mater.* **2013**, *69*, 195.
[13] C. Cheng, A. H. W. Ngan, *ACS Nano* **2015**, *9*, 3984.
[14] J. Weissmüller, D. Kramer, *Langmuir* **2005**, *21*, 4592.
[15] J. Weissmüller, J. W. Cahn, *Acta Mater.* **1997**, *45*, 1899.
[16] J. Weissmüller, H.-L. Duan, D. Farkas, *Acta Mater.* **2010**, *58*, 1.
[17] One can show that the closed- and open-circuit Young's moduli are related by $\left.\frac{dT}{d\varepsilon^*}\right|_E = \left.\frac{dT}{d\varepsilon^*}\right|_{q^V} - c^V(\varsigma^*)^2$. With the experimental data for the volume-specific capacitance c^V and for the coupling coefficient ς^* of our material, the two elastic constants are found to differ relatively by less than 10^{-4}.
[18] H.-J. Jin, S. Parida, D. Kramer, J. Weissmüller, *Surf. Sci.* **2008**, *602*, 3588.
[19] H.-J. Jin, J. Weissmüller, *Adv. Eng. Mater.* **2010**, *12*, 714.
[20] L. H. Shao, H. J. Jin, R. N. Viswanath, J. Weissmüller, *Europhys. Lett.* **2010**, *89*, 66001.
[21] N. Mameka, J. Markmann, H.-J. Jin, J. Weissmüller, *Acta Mater.* **2014**, *76*, 272.
[22] X. Y. Lang, H. T. Yuan, Y. Iwasa, M. W. Chen, *Scr. Mater.* **2011**, *64*, 923.
[23] G. Kaye, T. Laby, *Tables of Physical and Chemical Constants*, Longman, Harlow, UK **1995**.
[24] Y. Umeno, C. Elsässer, B. Meyer, P. Gumbsch, M. Nothacker, J. Weissmüller, F. Evers, *Europhys. Lett.* **2007**, *78*, 13001.
[25] M. Smetanin, Q. Deng, J. Weissmüller, *Phys. Chem. Chem. Phys.* **2011**, *13*, 17313.
[26] M. C. Lafouresse, U. Bertocci, C. R. Beauchamp, G. R. Stafford, *J. Electrochem. Soc.* **2012**, *159*, H816.
[27] Q. Deng, J. Weissmüller, *Langmuir* **2014**, *30*, 10522.
[28] S. Cattarin, D. Kramer, A. Lui, M. M. Musiani, *J. Phys. Chem. C* **2007**, *111*, 12643.
[29] Y. Saito, H. Takao, T. Tani, T. Nonoyama, K. Takatori, T. Homma, T. Nagaya, M. Nakamura, *Nature* **2004**, *432*, 84.
[30] A. M. Hodge, R. T. Doucette, M. M. Biener, J. Biener, O. Cervantes, A. V. Hamza, *J. Mater. Res.* **2009**, *24*, 1600.
[31] L. J. Gibson, M. F. Ashby, *Cellular Solids*, 2nd ed., Pergamon Press, Oxford, **1999**.
[32] B.-N. D. Ngô, A. Stukowski, N. Mameka, J. Markmann, K. Albe, J. Weissmüller, *Acta Mater.* **2015**, *93*, 144.
[33] L. Lührs, C. Soyarslan, J. Markmann, S. Bargmann, J. Weissmüller, *Scr. Mater.* **2016**, *110*, 65.
[34] S. Trasatti, O. A. Petrii, *Pure Appl. Chem.* **1991**, *63*, 711.
[35] P. S. Germain, W. G. Pell, B. E. Conway, *Electrochim. Acta* **2004**, *49*, 1775.
[36] Z. Shi, J. Lipkowski, M. Gamboa, P. Zelenay, A. Wieckowski, *J. Electroanal. Chem.* **1994**, *366*, 317.